Imaging Calcium Concentration Dynamics in Small Neuronal Compartments

Ryohei Yasuda,[1] Esther A. Nimchinsky,[1,3] Volker Scheuss,[1] Thomas A. Pologruto,[1,2] Thomas G. Oertner,[1,4] Bernardo L. Sabatini,[1,5] and Karel Svoboda[1*]

(Published 10 February 2004)

[1]Howard Hughes Medical Institute, The Cold Spring Harbor Laboratory, 1 Bungtown Road, Cold Spring Harbor, NY 11724, USA. [2]Graduate Program in Biophysics, Harvard University, Cambridge, MA 02138, USA. [3]Present address: Center for Molecular and Behavioral Neuroscience Aidekman Research Center, Rutgers State University, Newark Campus, 197 University Avenue, Newark, NJ 07102, USA. [4]Present address: Friedrich Miescher Institute, WRO-1066.4.10, Maulbeerstrasse 66, CH-4058 Basel, Switzerland. [5]Present address: Department of Neurobiology, Harvard Medical School, Boston, MA 02115, USA.

*Corresponding author. Telephone, 516-367-6878; fax, 516-367-8866; e-mail, svoboda@cshl.edu

Abstract

Calcium and its regulation play central roles diverse physiologic processes. Quantification of calcium concentrations ($[Ca^{2+}]$) in small neuronal compartments is crucial to understanding Ca^{2+}-dependent signaling. Here, we describe techniques that are optimized for two-photon imaging of $[Ca^{2+}]$ dynamics in small compartments such as dendrites and dendritic spines.

Introduction

Ca^{2+} influx into spines and dendrites triggers diverse signaling pathways underlying adaptive neuronal responses. Ca^{2+} accumulations are required to induce most forms of long-term potentiation and depression, putative mechanisms of memory and learning (*1*, *2*). Ca^{2+} also plays essential roles in the regulation of Ca^{2+} channels (*3*–*5*), dendritic growth (*6*), and spine formation (*7*, *8*), as well as in decisions about cell death and survival (*9*). A fundamental question in neuronal signaling is how Ca^{2+} can play roles in pathways leading to such diverse outcomes. To begin to decipher specificity in Ca^{2+} signaling, quantitative measurements of calcium concentration ($[Ca^{2+}]$) dynamics, especially transient changes in $[Ca^{2+}]$ ($[Ca^{2+}]$ transients), with high temporal and spatial resolutions are crucial. Imaging methods can probe $[Ca^{2+}]$ dynamics with submicrometer spatial and submillisecond temporal resolutions.

Here, we describe detailed Ca^{2+} imaging methods, as well as illustrative experiments that were performed on dendrites and dendritic spines of CA1 pyramidal neurons in rat acute hippocampal brain slices. Dendritic spines, the sites of most excitatory synapses, are small protrusions emanating from dendrites. Spines typically consist of a small head (volume ~ 0.1 μm^3) connected to dendrites by a thin neck (diameter = 0.1 μm). The spine neck acts as a diffusion barrier, isolating biochemical reactions in spines from their parent dendrites and other spines (*10*–*13*). Ca^{2+} imaging methods employing synthetic Ca^{2+}-sensitive fluorescent indicators have been used to study the mechanisms shaping Ca^{2+} signals in spines. In CA1 pyramidal neurons, weak synaptic stimuli produce Ca^{2+} elevations largely restricted to spine heads where activated synapses terminate. These local changes in $[Ca^{2+}]$ are due to Ca^{2+} entering the cell predominantly through *N*-methyl-D-aspartate (NMDA) receptors (NMDARs) (*14*–*18*). In contrast, induction of action potentials (APs) propagating from the cell body into dendrites (back-propagating APs) causes Ca^{2+} influx through voltage-sensitive Ca^{2+} channels (VSCC) (*5*, *11*, *19*, *20*).

In addition to Ca^{2+} influx, extrusion and buffering also shape spine Ca^{2+} signals. Small dendritic branches and their spines are characterized by powerful extrusion mechanisms and low Ca^{2+} buffering capacities, facilitating very fast (~ 10 ms) Ca^{2+} clearance from spines (*21*). Because diffusional coupling between spines and their parent dendrites is weak [> 100 ms; (*11*)], spine Ca^{2+} does not diffuse into the dendrite or further to other spines.

Spine Ca^{2+} signals are also of interest because they can be used to monitor the function and plasticity of individual synapses. NMDAR-mediated increases in $[Ca^{2+}]$ have been used to image the stochastic release of glutamate from individual synaptic terminals (*15*, *17*–*19*, *22*, *23*). In addition, spine Ca^{2+} signals can be used to examine the function of particular Ca^{2+}-permeable receptors and channels. This information then allows measurement of the occupancy of NMDARs (*15*) and determination of the number of voltage-gated channels (*5*, *20*) and NMDARs (*24*) opening in individual spines with single-channel resolution.

Like most experiments on neurons, imaging changes in neuronal $[Ca^{2+}]$ are best performed in preparations that are as intact as possible, such as brain slices or even the intact brain. Experiments on these types of samples are facilitated by the use of two-photon laser scanning microscopy (2PLSM) (*25*, *26*), and as a consequence the methods introduced here are optimized for this imaging modality. However, these techniques can be easily adapted to other imaging techniques and preparations, such as confocal imaging of dissociated cultured neurons (*22*).

Materials

0.22 μm centrifugal filter (Ultrafree-MC; Millipore, Bedford, MA)

Sprague Dawley rat

Chemicals and Reagents

(-)-Bicuculline methiodide (bicuculline; Tocris, Ellisville, MO, #0109)

$CaCl_2$

Choline chloride

DL-2-Amino-5-phosphonovaleric acid (D-APV; Tocris, Ellisville, MO, #0105)

Note: This may only be required for troubleshooting.

3-((*R*)-2-Carboxypiperazin-4-yl)-propyl-1-phosphonic acid (R-CPP; Tocris, #0247)

Note: This may only be required for troubleshooting.

D-glucose

Dimethylsulfoxide (DMSO; Fluka, Switzerland, #41648)

Disodium adenosine 5′-triphosphate (Na_2-ATP; Sigma-Aldrich, #A2383)

Disodium guanosine 5′-triphosphate (Na_2-GTP; Sigma-Aldrich, #G8877)

D-serine (Sigma-Aldrich, #S4250)

Hepes (Sigma-Aldrich)

Isoflurane (Baxter, Deerfield, IL)

KCl

$MgCl_2$

$MgSO_4$

$NaHCO_3$

NaH_2PO_4

NaCl

2,3-Dioxo-6-nitro-1,2,3,4-tetrahydrobenzo[f]quinoxaline-7-sulfonamide (NBQX; Tocris, Ellisville, MO, #0373)

O_2/CO_2 (95% O_2 and 5% CO_2) tank

Sodium L-ascorbic acid (Sigma-Aldrich, #A7631)

Sodium phosphocreatine (Sigma-Aldrich, #P7936)

Sodium pyruvic acid (Sigma-Aldrich, #P8574)

Equipment

Solution Preparation

Vapor pressure osmometer (Vapro; Wesco Inc., Logan, UT, 84321)

Slice Preparation

Slice chamber [such as that described in (*27*)]

Slice incubation chamber [for example, see (*27*)]

Vibrating tissue slicer (such as Vibratome; TPI, St. Louis, MO)

Water bath set at 34°C

Electrodes

Glass capillary tubing for patch pipettes (borosilicate standard wall with filament, outer diameter = 1.5 mm, inner diameter = 0.86 mm; Warner Instruments, #G150F-3)

Glass capillary tubing for extracellular stimulation pipettes (borosilicate thin wall with filament, outer diameter = 1.5 mm, inner diameter = 1.15 mm; Warner Instruments, #G150TF-4)

Microforge (Narishige, Tokyo, #MF-900)

Pipette puller for extracellular stimulation pipette (such as Davis Kopf, Tujunga, CA, #700 D)

Pipette puller for patch pipette (such as Sutter, Novato, CA, #P-2000)

Microscope

2PLSM (Fig. 1).

Note: Suitable instruments can be turnkey (for example, Bio-Rad or Zeiss), based on a modified commercial confocal microscope (29), or completely custom-built (30, 31). In each, it is critical to optimize the efficiency of the fluorescence detection system (26, 30).

High-magnification lens [such as 60×, numerical aperture (N.A.) > 0.8]

Infrared differential interference contrast (IRDIC) or Dodt contrast (IRDC) in whole field mode for whole cell recordings (*32*)

Laser scanning Dodt contrast (LSDC; Fig. 1) or differential interference contrast (LSDIC) (*30*) microscope

Note: Fig. 1 illustrates how high-contrast LSDC and two-photon fluorescence can be imaged simultaneously. This simultaneous imaging is crucial for the precise placement of focal stimulating electrodes (30).

Low-magnification objective (such as 4× to 5×)

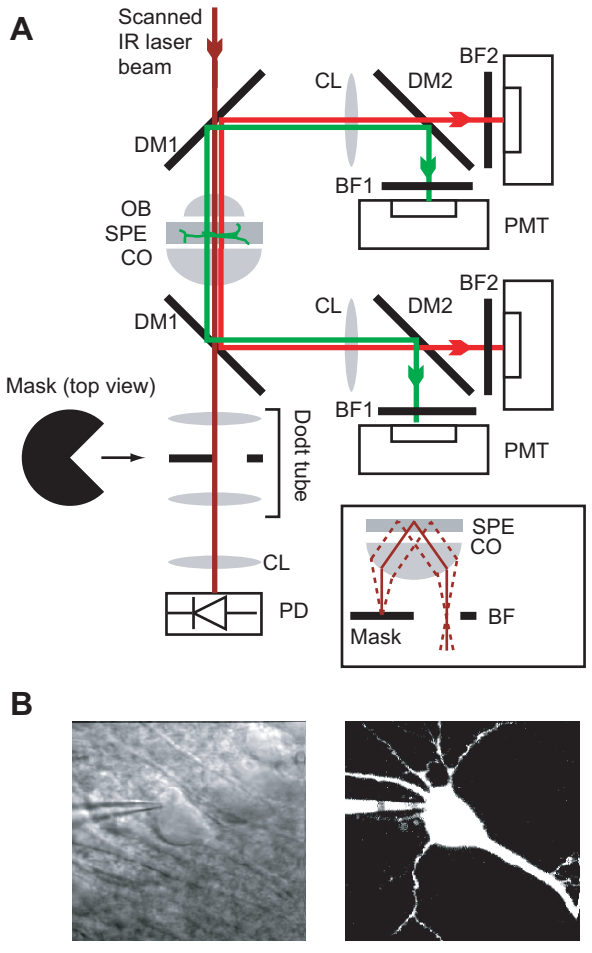

Fig. 1. Schematic of the 2-photon microscope with laser scanning Dodt contrast (LSDC). (**A**) Specimen (SPE) is excited with a Ti:sapphire laser (brown) running at a wavelength of ~ 810 nm (repetition rate, 76 MHz; pulse width, 100 fs). Epi- and transfluorescence (green, red) are collected through the objective (OB) and condenser (CO), respectively. Fluorescence photons are reflected by dichroic mirrors (DM1, 700 nm longpass) into detection systems consisting of collection lenses (CL) that image the respective back apertures onto photomultipliers tube detectors (PMT, R3896, Hamamatsu, Japan). Dichroic mirrors (DM2, typically 565 nm longpass) and bandpass filters (BF1 and BF2, typically BGG22 and Q607/45, respectively; all from Chroma, Rockingham, VT) separate the signals from the red and green fluorophores. In addition, the laser light passing through the sample is collected through a Dodt tube (*60, 61*) and is detected by a photodiode (PD). The Dodt tube consists of a 1:1 telescope, which generates an intermediate image of the condenser back aperture onto a mask (for example, a quarter annulus). Therefore, the mask is at a plane reciprocal to the specimen plane, admitting only light scattered into certain angles (inset). If this laser light is collected during scanning, a high-contrast image can be obtained. Dodt gradient contrast has important advantages compared to DIC microscopy. First, there are no additional optical surfaces in the 2PLSM fluorescence path. Second, a DIC prism is not required. The DIC prism is expensive and degrades the point spread function of 2PLSM. (**B**) Simultaneously acquired 2PLSM (right) and LSDC (left) images.

Electrophysiology Setup for Whole-Cell Voltage Clamp Recording

Harp [U-shaped gold wire (Premion; diameter = 0.5 mm; Alfa Aesar, Ward Hill, MA) strung with several strands of fine thread (*28*)]

Note: The size of the harp should be a little larger than a slice.

Micromanipulator for patch clamp recordings (such as Sutter, #MP-285)

Micromanipulator for synaptic stimulation (Sutter, #MP-285)

Note: For stable focal stimulation, it is important to use motorized manipulators with large movement ranges and excellent stability.

Patch clamp amplifier (such as Axopatch 200B; Axon Instruments, Union City, CA)

Stimulus isolation unit (such as Iso-flex; A.M.P.I., Jerusalem, Israel)

Temperature controller (Warner Instruments, #TC-324B)

Recipes

Recipe 1: Cutting Solution

$NaHCO_3$	25 mM
D-glucose	25 mM
$MgSO_4$	7 mM
KCl	2.5 mM
NaH_2PO_4	1.25 mM
$CaCl_2$	0.5 mM

Store at 4°C. Within 3 days of use, add:

Choline chloride	110 mM
Sodium L-ascorbic acid	11.6 mM
Sodium pyruvic acid	3.1 mM

Bubble with O_2/CO_2 for at least 10 min and chill to <4°C before use.

Recipe 2: Artificial Cerebrospinal Fluid (ACSF)

NaCl	127 mM
$NaHCO_3$	25 mM
D-glucose	25 mM
KCl	2.5 mM
NaH_2PO_4	1.25 mM
$MgCl_2$	1.0 mM

Bubble with O_2/CO_2. Adjust pH to 7.25 to 7.35 (25°C), and the osmolarity to 300 to 310 mOsm after addition of $CaCl_2$ using vapor pressure osmometer. Store at 4°C.

On day of use, bubble with O_2/CO_2. Then add:

$CaCl_2$	2.0 mM

Recipe 3: Indicator Stock

Prepare 10 to 20 mM of the Ca^{2+} indicator in dH_2O or Patch Pipette Internal Solution (Recipe 4). Store 1- to 2-μl aliquots at –20°C for up to one year.

Recipe 4: Patch Pipette Internal Solution

$KMeSO_3$ (or $CsMeSO_3$)	130 mM
Hepes	10 mM
Sodium phosphocreatine	10 mM
$MgCl_2$	4 mM
Na_2-ATP	4 mM
Na_2-GTP	0.4 mM
Sodium L-ascorbic acid	3 mM
Indicator Stock (Recipe 3)	Variable

Prepare 50 to 250 ml. Adjust pH to 7.25 to 7.35 (25°C) with KOH (or CsOH) and osmolarity to 290 to 310 mOsm using vapor pressure osmometer. Store in 0.5-ml aliquots at –20°C.

Dilute Indicator Stock (Recipe 3) to desired final concentration in ~ 0.5-ml volumes, filter with a 0.22 μm pore centrifuge filter, and freeze in aliquots appropriate for 1 day of experiments (for example, 20 μl; 1 μl per patch pipette is sufficient).

Note: The choice of indicator and its concentration will depend on the experimental question. Different indicators differ in their affinities for Ca2+ and other variables. As a rough guide, we recommend 100 to 300 mM Fluo-4, Fluo-5F, X-Rhod-1, or X-Rhod-5F to measure AP-evoked Ca2+ dynamics, and 500 mM Fluo-4FF, X-Rhod-FF, or Rhod-FF to detect changes in [Ca2+] evoked by synaptic stimulation. Further discussion of indicator choice, including use of single and dual indicators, can be found in "Choosing a Ca2+-Sensitive Indicator," in "Notes and Remarks," below.

Recipe 5: NBQX

Prepare 10 to 20 mM NBQX in dH_2O. Store aliquots at –20°C.

Recipe 6: Bicuculline

Prepare 10 to 30 mM bicuculline in DMSO. Store aliquots at –20°C.

Recipe 7: D-Serine

Prepare 10 to 20 mM D-serine in dH_2O. Store aliquots at –20°C.

Note: This may only be required if troubleshooting is necessary.

Recipe 8: D-CPP

Prepare 10 to 20 mM D-CPP in dH_2O. Store aliquots at –20°C.

Note: This may only be required if troubleshooting is necessary.

Recipe 9: D-APV

Prepare 10 to 20 mM D-APV in dH_2O. Store aliquots at –20°C.

Note: This may only be required if troubleshooting is necessary.

Instructions

Slice Preparation

1. Anesthetize rat with isoflurane.
2. Decapitate rat.
3. Rapidly remove desired block of tissue and place in ice-cold Cutting Solution (Recipe 1).
4. Mount block on platform of vibrating tissue slicer.

   Note: The dendrites of the neurons of interest should run close to parallel to the slice surface.
5. Cut 300- to 350-μm-thick slices and place them immediately in a slice chamber at 34°C in ACSF (Recipe 2).
6. Incubate slices for 45 to 60 min at 34°C and then maintain at room temperature.

Imaging [Ca^{2+}] Transients Evoked by APs

AP-evoked [Ca^{2+}] transients are detected by 2PLSM with the appropriate Ca^{2+} indicator. Whole-cell recordings are made from neurons in brain slices. The patch electrode delivers the dye and allows the cell to be stimulated. 2PLSM scanning detects changes in fluorescence associated with changes in [Ca^{2+}]. For each stimulus trial, measure the dark current of the photomultiplier (PMT), the fluorescence at resting [Ca^{2+}], and the fluorescence after stimulation.

1. Place a slice into recording chamber and secure with harp.
2. Let slice settle for 15 to 30 min before recording to minimize the movement of the slice during the recording.
3. Visualize neurons by IRDIC or IRDC.
4. With an electrode (resistance ~ 4 to 6 MΩ) containing K^+-based Patch Pipette Internal Solution (Recipe 4) made with the desired Ca^{2+} indicator (see "Choosing a Ca^{2+}-Sensitive Indicator," in "Notes and Remarks," below), patch neurons with somata ~ 40 μm below the slice surface.

   Note: A low-access resistance (<20 MW) is crucial for good dye loading. However, access resistance that is too low (<10 MW) may cause degraded VSCC-mediated responses, possibly due to washout of some critical cellular component. To minimize background fluorescence caused by indicator spilled from the pipette, approach the cell with the patch pipette as quickly as possible and keep the pressure applied to the pipette tip low (~ 0.3 psi). If using a single indicator, it may be advisable to fill the very tip of the electrode with indicator-free internal solution, so that indicator is not ejected into the tissue while approaching the neuron (see "Quantification of [Ca2+] Transients with a Single Indicator," below).
5. After establishing a whole-cell recording, wait for ~ 20 min for indicator loading. Continually check the time course of fluorescence intensity to monitor the state of indicator loading.
6. Using 2PLSM, identify suitable structures (such as spines and dendrites) relatively close (< 150 μm) to the soma (Fig. 2).

   Note: At greater distances, the propagation of APs is not reliable (33), and diffusional equilibration does not occur over the time scale of the experiment.
7. Use 2PLSM linescans intersecting a spine and dendrite (Fig. 2, C and D).

   Note: During scanning, expose the sample to light as little as possible.
8. A typical trial starts with a measurement of the dark current of the photo-multiplier (0 to 50 ms) followed by shutter opening. After a short measurements of baseline fluorescence (60 to 120 ms), action potential is evoked by somatic current injection (1 to 3 nA, 2 ms) through the pipette. Measurement of peak fluorescence is averaged over 3 to 20 ms around the peak (Fig. 2, D and E).

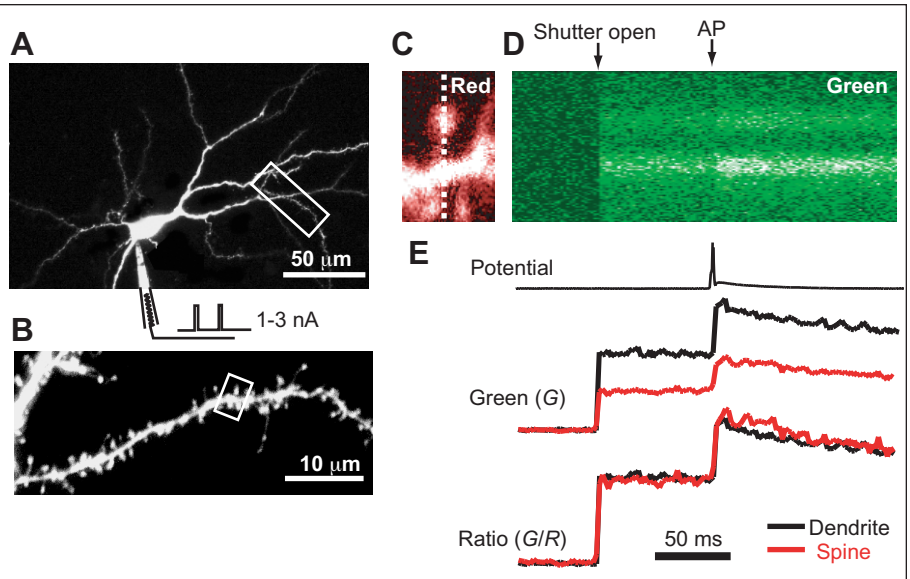

Fig. 2. Measurement of changes in [Ca^{2+}] evoked by APs. (**A**) 2PLSM image of a hippocampal CA1 neuron. (**B**) Dendritic region (box in A). (**C**) Spines (box in B). Neurons were loaded with a green Ca^{2+} indicator (300 μM Fluo-5F) and a red Ca^{2+}-insensitive dye (30 μM Alexa-594). (**D**) Green fluorescence during linescan (dashed line in C). Horizontal axis indicates time. (**E**) Time courses of membrane potential (top) and green fluorescence, *G* (middle) (red, spine; black, dendrite). The ratio *G*/*R* is obtained by dividing *G* by red fluorescence averaged over the entire exposure time (60 to 250 ms). Note that the shutter was opened with a delay, which allows the measurement of the dark current level during each trial and minimizes light exposure.

Imaging [Ca^{2+}] Transients Evoked by Synaptic Stimulation

Preparation of stimulating electrode

1. Pull a sharp micropipette with a long taper.
2. Using a microforge, bend the last 200 μm of the electrode to an angle such that when mounted in the pipette holder, it will approach the surface of the slice (Fig. 3A) perpendicularly, allowing the pipette to be positioned vertically without compressing the tissue.
3. Break off the tip of the electrode, leaving a tip diameter of 2 to 3 μm.
4. Fill electrode with 1 M NaCl.

Electrophysiology and imaging

1. Place a slice into the recording chamber, as described above.
2. If applicable, block AMPA and $GABA_A$ receptors by adding NBQX (Recipe 5) and Bicuculline (Recipe 6) at a final concentration of 10 μM to the ACSF.
3. Visualize neurons by IRDIC or IRDC.
4. Position the stimulating electrode over the soma of the targeted neuron.
5. Move it approximately 1 mm away to prevent collisions with the recording electrode.
6. With an electrode (4 to 6 MΩ) containing Cs^+- (for voltage-clamp experiments) or K^+-based (for current-clamp experiments) Patch Pipette Internal Solution (Recipe 4) made with the desired Ca^{2+} indicator, patch neurons with somata 40 μm below the slice surface, with apical dendrites parallel to the slice surface.

   Note: A low-access resistance (<20 MW) is crucial for good indicator loading. To minimize background fluorescence caused by indicator spilled from the pipette, approach the cell with the patch pipette as quickly as possible and keep the pressure applied to the pipette tip low (~ 0.3 psi).
7. If working at the reversal potential of the NMDAR, depolarize the somatic membrane potential until the synaptic current reverses (range 0 to 20 mV, depending on the distance from the synapse to the soma).
8. Return the stimulating electrode to its position above the patched soma.

9. With 2PLSM, find suitable dendritic segments with a number of spines.

   Note: For quantitative measurements, it is crucial to restrict imaging to dendrites within ~ 150 mm of the soma, because at sites farther than that in the dendritic tree, diffusional equilibration does not occur. Furthermore, at greater distances, voltage control is difficult.

10. Using LSDC or LSDIC, place tip of stimulating electrode within 5 to 20 μm of the targeted dendritic segment (Fig. 3, A and B).

    Note: Placing the electrode closer than 5 mm increases the likelihood of direct depolarization of the membrane. Placing it farther than 20 mm reduces the chance of stimulating an axon impinging on the imaged dendrite. Try to avoid imaging through the stimulating electrode. The addition of a red Ca^{2+}-insensitive fluorophore to the Ca^{2+}-sensitive indicator helps to visualize the structure of the target dendrite (Fig. 3, B and C).

11. During the acquisition of an image (5 frames, ~ 100 ms each), open the shutter between frames 1 and 2, and stimulate with paired pulses (0.1 to 10 V, 0.1 to 0.5 ms) between frames 3 and 4.

    Note: Pair pulses enhance the probability of release (34), and, therefore, of a response.

12. Measure the difference (ΔG, Figs. 3 C and D) between the image before stimulation (frame 3) and after (frame 4) online.

    Note: Stimulated synapses can be seen as bright regions corresponding to dendritic spines (Fig. 3D).

13. While repeating steps 11 and 12 at 5-s intervals, change the stimulus voltage until an active synapse is found.

14. If necessary, move the stimulating electrode in the axial direction between trials until an active synapse is found.

15. If no active synapse is found, raise the stimulating electrode out of the tissue, move a few microns laterally, and try again.

16. If an active synapse is found, increase the stimulation voltage by ~ 20% to avoid stimulation failures, and collect data.

    Note: Start collecting data no less than 20 min after whole-cell recording.

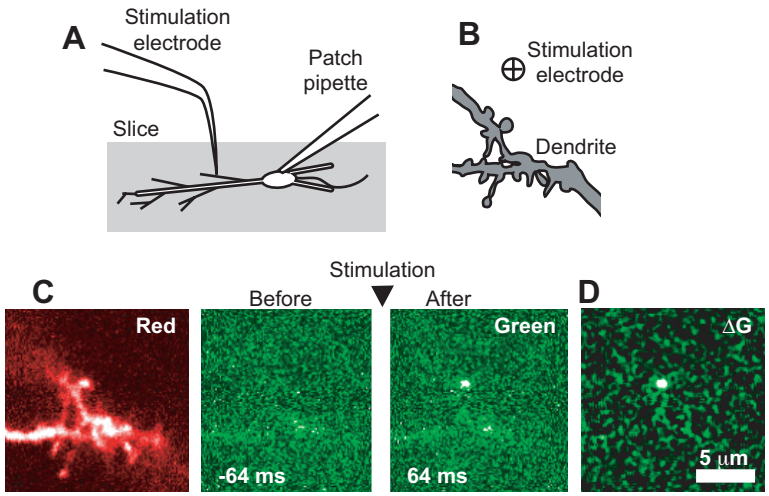

Fig. 3. Measurement of changes in $[Ca^{2+}]$ evoked by synaptic stimulation. (**A** and **B**) Schematic of the experiment. Paired-pulse stimuli (0.2 to 5 V, 0.2 ms, interstimulus interval 20 ms) are applied with an extracellular glass stimulation pipette. The stimulation electrode is bent so that the tip enters the slice perpendicular to the surface. This allows positioning of the stimulus electrode tip close to the target dendrite with minimal mechanical perturbation. (**C**) The red Ca^{2+}-insensitive dye (30 μM Alexa-594) helps in visualization of small structures. The green Ca^{2+} indicator (300 μM Fluo-5F) is very dim at rest, but shows large fluorescence changes in activate spines (compare before and after). (**D**) Difference (ΔG) image.

Troubleshooting

Slice Quality

Slices should be used as soon as possible after the rest period. If there is evidence of unhealthy slices, such as crinkled neuronal surfaces, prominent nuclei, or an abundance of dead cells, it is better to discard the slices and cut fresh ones.

Small Fluorescence Change in Response to an AP

100 μM Fluo-4 or Fluo-5F applied to pyramidal neurons should result in greater than 50% increases in fluorescence in response to single APs. Response can be smaller for several reasons:

(i) ATP is required to prevent Ca^{2+} channels from running down, that is, losing responsiveness over time (*35*). Make sure that a saturating concentration of ATP is in the internal solution and use fresh aliquots.

(ii) Very-low-access resistance (<10 MΩ) patch recordings can lead to degradation of VSCC-mediated responses, possibly due to washout of some critical chemicals.

(iii) AP propagation can be unreliable at distal (> 100 μm) spines and dendrites (*33*). Image proximal spines and dendrites.

(iv) Spilling indicator in the extracellular space increases background fluorescence, decreasing the signal-to-noise ratio. When the patch pipette is in the slice, keep the pipette pressure low (< 0.3 psi) and patch as quickly as possible. These precautions will also prevent the cells from firing trains of APs due to high K^+ in the extracellular medium. Firing of APs can lead to depression of VSCCs (*5*).

(v) Ca^{2+} indicators act as buffers, thus large indicator concentrations may lead to small signals (see "Notes and Remarks," below, for further discussion).

(vi) A local or global increase in resting [Ca^{2+}] may reduce the measured ratio of the transient fluorescence response to the baseline fluorescence ($\Delta F/F_o$) (see Table 1 for a list of symbols and abbreviations). Increased resting [Ca^{2+}] should be immediately evident as a change in the baseline. For example, the ratio of the Ca^{2+}-sensitive to Ca^{2+}-insensitive fluorescence intensities should increase or, if a single Ca^{2+}-sensitive indicator is used, the baseline fluorescence should rise (see "Notes and Remarks," below, for further discussion).

(vii) Phototoxicity can lead to local or global degradation of the health of the cell and can also produce a fluorescent deposit that contributes to baseline fluorescence. To avoid phototoxicity, image only as long as absolutely necessary and determine the lowest laser intensity that can generate the necessary signal-to-noise ratio (SNR).

Problems in Imaging [Ca^{2+}] Transients Evoked by Synaptic Stimulation

Tissue health

The search for [Ca^{2+}] transients evoked by synaptic stimulation can be time consuming. Ideally, one wants to start collecting data no less than 20 min after patching the neuron, because it is important to allow the local indicator concentration to reach steady state. (If the indicator concentration changes during the experiment, the amplitude of Ca^{2+} responses will change as a result.) However, because the health of the tissue is crucial, it is also difficult to record from a neuron for much longer than an hour. Therefore, depending on the nature of the planned experiment (number of trials required, wash-in and equilibration of drugs, washout), it may not be advisable to persist in trying to find an active synapse 30 to 40 min after patching; instead, patch a fresh neuron.

Absence of response

The flow chart (Fig. 4) describes multiple tests to diagnose the cause of the lack of response and the appropriate action to take once the problem is identified.

Nature of the response

If the stimulating electrode is too close (<5 μm) to the imaged segment, signals due to direct depolarization of the postsynaptic neuron may occur. These responses can be recognized because the signal will extend spatially beyond a single spine without failures. Additional tests include application of NMDAR antagonists, such as D-APV (50 μM) or D-CPP (10 μM); if the signals disappear completely, they were likely synaptic.

Loss of synaptic responses

Unstable [Ca^{2+}] responses can be due to several factors:

(i) Movement of the slice. This can be prevented by using an appropriately shaped harp.

(ii) Movement of the stimulating electrode. The requirements for the mechanical stability of the stimulating electrode holder are as stringent as those for the patch electrode. Use a high-quality manipulator. Test for drift of the electrode relative to the slice chamber.

(iii) Receptor desensitization or downregulation. There are several forms of desensitization for NMDAR. Addition of 50 μM D-serine to the bath will prevent the glycine-dependent form of desensitization (*36*). For problems caused by increases in resting [Ca^{2+}] or photodamage, see the solutions to these issues described in "Small Fluorescence Change in Response to an AP."

Table 1: Symbols and abbreviations.

Symbols	Unit	Description
$[Ca^{2+}]$	M	Free Ca^{2+} concentration
$[Ca^{2+}]_o$	M	Resting $[Ca^{2+}]$
$[Ca^{2+}]_T$	M	Total (free and bound) $[Ca^{2+}]$
B		Endogenous buffer
b_{ex}	m^{-3}	Background fluorescence outside compartment per unit volume
b_{sp}	m^{-3}	Background fluorescence inside compartment per unit volume
$e(t)$	mol/s	Ca^{2+} efflux from a compartment
f	m^{-3}	Fluorescence after stimulation per unit volume
f_o	m^{-3}	Fluorescence of baseline per unit volume
F		Fluorescence
F_B		Background fluorescence
$F_{o,\,raw}$		Raw fluorescence of baseline
F_o		Baseline fluorescence
F_{max}		Fluorescence intensity at saturating $[Ca^{2+}]$
F_{min}		Fluorescence intensity at zero $[Ca^{2+}]$
G		Green fluorescence
G_o		Baseline green fluorescence
$i(t)$	mol/s	Ca^{2+} current into a compartment
K_D or $K_D^{(dye)}$	M	Dissociation constant of $[Ca^{2+}]$ indicator
$K_D^{(B)}$	M	Dissociation constant of endogenous buffer
N		Number of photons detected
NL		Nonlinearity of fluorescence response
Q	mol	Amount of Ca^{2+} ions transferred
R		Red fluorescence
SNR		Signal-to-noise ratio
V_{ex}	m^3	Excitation volume outside compartment
V_{sp}	m^3	Volume of dendritic spine
ΔF		Transient fluorescence response
ΔG		Transient green fluorescence response
Γ	s^{-1}	Extrusion rate constant
κ_B		Buffer binding ratio of endogenous buffers
κ_{dye}		Buffer binding ratio of the Ca^{2+} indicator
τ_{NMDA}	s	Time constant of NMDAR current

Notes and Remarks

Loading Cells with Ca^{2+} Indicator

Various methods have been used to load neurons with Ca^{2+} indicators. Bulk loading methods based on indicators conjugated to acetoxymethyl esters (*37*, *38*) and dextrans (*39*, *40*) are convenient, but they do not allow precise control of the quantity of the indicator in the cellular cytoplasm. In addition, these Ca^{2+} indicators tend to partition into poorly defined intracellular compartments, compromising the quantitative interpretation of fluorescence measurements. Neurons can be loaded with Ca^{2+} indicators by microinjection and iontophoresis through sharp electrodes (*41*, *42*), which allows somewhat better, but still limited, control of the cytoplasmic indicator content. Whole-cell recording methods, in which the cell cytoplasm is allowed to equilibrate with the pipette solution, are preferred for quantitative measurements (*11*, *43-46*) and should be used whenever possible.

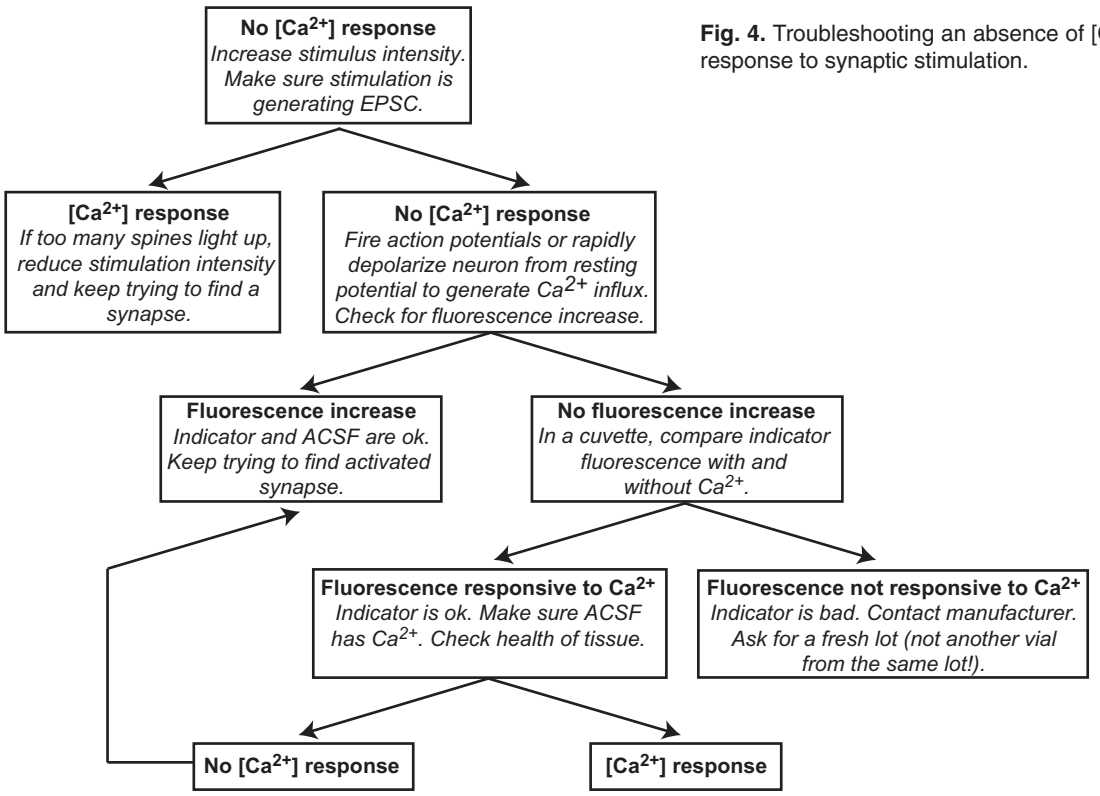

Fig. 4. Troubleshooting an absence of [Ca^{2+}] transient in response to synaptic stimulation.

Choosing a Ca^{2+}-Sensitive Indicator

A standard Ca^{2+} sensor consists of a fluorophore coupled to a Ca^{2+} buffer, such as ethylenedioxybis(o-phenylenenitrilo)tetraacetic acid (BAPTA) (*47*). Ca^{2+} binding to the buffer changes the fluorescence properties of the indicator. A large number of Ca^{2+} indicators that differ in the affinity for Ca^{2+} and dynamic range have become available. The choice of the most appropriate indicator must be made on the basis of the particular scientific question. Here, we discuss factors that influence the choice of Ca^{2+} indicator for certain types of measurements.

Some Ca^{2+}-sensitive indicators, such as Fura-2, change absorption and emission spectra upon Ca^{2+} binding. These indicators allow calibration of absolute [Ca^{2+}] independent of focal position, geometrical factors, and photobleaching by "ratiometric" measurements (*48*). However, because of SNR considerations, we do not consider ratiometric measurements practical in small cellular compartments.

Instead, we employ single-wavelength measurements with selected Ca^{2+} indicators with large dynamic ranges. These indicators can be used in combination with Ca^{2+}-insensitive dyes to perform dual color measurements (Figs. 2 and 3). Numerous variants of indicators with suitable properties are available, such as the Fluo, Rhod, and Oregon green BAPTA (OGB) families (from Molecular Probes). Members of these families cover a broad range of Ca^{2+} binding affinities.

Maximizing SNR

Typically, the Ca^{2+} response is quantified as $\Delta F/F_o$, where F_o is the baseline fluorescence, and ΔF is the transient fluorescence response above baseline. For measurements in small neuronal compartments, SNRs are fundamentally limited by stochastic fluctuations in the number of photons detected (N) (*20*). We define SNR as the ratio between the fluorescence signal (ΔF) and the shot noise on the baseline fluorescence ($\sim F_o/N^{1/2}$). Thus, the number of photons required for SNR ~ 1 is given by Eq. 1.

$$N > \left(\frac{\Delta F}{F_o}\right)^{-2} \quad \text{(Eq. 1)}$$

For example, for typical Fura-2 signals in response to single APs ($\Delta F/F_o \sim 0.05$) (*49*), SNR ~ 1 demands collection of hundreds of photons, whereas only a few photons will suffice for Fluo-4 ($\Delta F/F_o \sim 0.6$) (*20*). Therefore, for optimal SNR it is crucial to choose indicators and experimental conditions that maximize $\Delta F/F_o$.

Other important factors include the absorption cross-section and quantum efficiency, both of which contribute to *N*. Finally, an important consideration in choosing an indicator is phototoxicity and photobleaching. Fluorophores that are easily bleached also tend to be toxic to cells. Less toxic indicators can thus be excited more strongly, leading to better SNR. Unfortunately, little quantitative information is currently available on this important topic. On the basis of our experience, we would rank indicators as follows (keeping fluorescence intensity, not SNR, constant; from best to worst): Fura-2 > Fluo-4, -5F, and -4FF > OGB-1 > Fluo-3. We prefer Fluo-4, -5F, and -4FF; although the Fura indicators produce the greatest intensity, we have found the SNR of Fluo-4 and its relatives to be superior to that of the Fura family.

Affinity and dynamic range of the Ca^{2+} indicator

The fluorescence intensity of Ca^{2+} indicators is related to $[Ca^{2+}]$ as defined by Eq. 2, where F_{max} and F_{min} are the fluorescence intensities at saturating and zero Ca^{2+} concentrations, respectively, and K_D is the dissociation constant (Fig. 5).

$$\frac{F - F_{min}}{F_{max} - F_{min}} = \frac{[Ca^{2+}]}{[Ca^{2+}] + K_D} \qquad \text{(Eq. 2)}$$

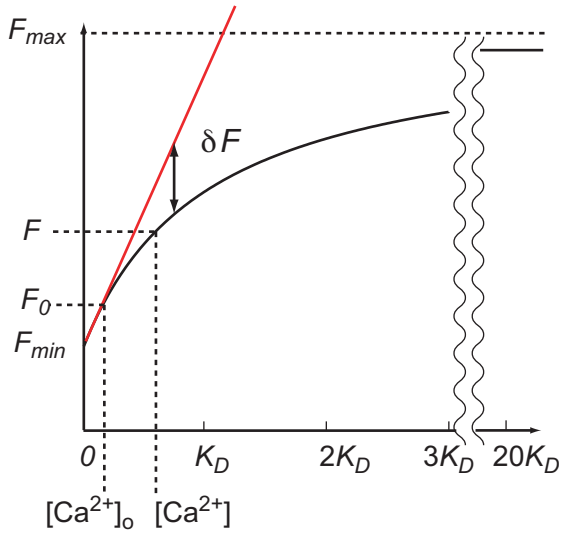

Fig. 5. Fluorescence of Ca^{2+} indicator as a function of $[Ca^{2+}]$. Curves correspond to the linear approximation (red; Eq. 3) and the exact curve (black; Eq. 2).

Choosing the correct K_D is important for high SNRs. If the K_D is too large (affinity is too low) compared to typical transient changes in $[Ca^{2+}]$, $\Delta F/F_o$ will be small. Conversely, if K_D is too small, transient changes in $[Ca^{2+}]$ (or perhaps even the resting $[Ca^{2+}]$) will saturate the dye, and $\Delta F/F_o$ will also be small. Furthermore, in this case $\Delta F/F_o$ will be a nonlinear function of $[Ca^{2+}]$, complicating the quantitative interpretation of the data (see *Linearity* below for further discussion). A large dynamic range, defined as F_{max}/F_{min}, is also important for good SNR (Eq. 1).

It is useful to calibrate the K_D and F_{max}/F_{min} of particular Ca^{2+} indicators. Because these parameters depend on ionic strength, pH, and temperature, they need to be measured when the indicators are dissolved in the internal solution (*50*). Briefly, $[Ca^{2+}]$ is clamped by 10 mM ethylene glycol-bis(2-aminoethylether)-N,N,N′,N′,-tetraacetic acid (EGTA) to different levels, and the relation between fluorescence and $[Ca^{2+}]$ is measured. $[Ca^{2+}]$ is computed by the MaxChelator program (*51*) (http://www.stanford.edu/ ~cpatton/maxc.html). To measure ranges of $[Ca^{2+}]$ larger than 1 μM, buffers are not required to set the $[Ca^{2+}]$. Table 2 summarizes measurements from our laboratory in K^+-based internal solution (listed as Recipe 4, for simplicity prepared without ATP, GTP, phosphocreatine, and ascorbic acid). These values are only a rough guide, because F_{max}/F_{min} can vary from batch to batch and is likely to be smaller in cells because of interactions between the indicators and cytoplasmic proteins (*46, 52, 53*). Similarly, the K_D may be larger in cells than when measured in cuvettes (*54*). Table 2 also includes expected values of $\Delta F/F_o$ evoked by single APs and synaptic stimuli in small CA1 dendrites and spines (*11*).

Indicator	K_D 24°C (μM)	K_D 34°C (μM)	$\frac{F_{max}}{F_{min}}$	AP (50 nM)		NMDA (1 μM)		κ_{Dye} (100 μM)
				$\frac{\Delta F}{F_o}$ (%)	*NL* (%)	$\frac{\Delta F}{F_o}$ (%)	*NL* (%)	
Green indicators								
OGB-1	0.38	0.21	10	40	48	300	500	310
Fluo-4	0.80	0.34	>40	>60	29	500	300	220
Fluo-5F	1.6	1.3	>40	>50	8	700	81	70
Fluo-4FF	10.4	8.1	>40	>20	1	>400	13	10
Red indicators								
X-Rhod-1	0.82	0.73	>40	60	14	700	144	120
X-Rhod-5F	1.9	2.3	>40	>40	4	700	46	40
X-Rhod-FF	24	23	>30	>6	0.4	>113	5	4
Rhod-FF	26	20	>40	>9	0.5	>68	5	5

Table 2: Properties of Ca^{2+} indicators. Typical response ($\Delta F/F_o$) and *NL* for AP-evoked $\Delta[Ca^{2+}]$ (AP; $\Delta[Ca^{2+}]$ = 50 nM, $[Ca^{2+}]_o$ = 50 nM, 34°C) and for synaptic stimulation-evoked $\Delta[Ca^{2+}]$ (NMDA; $\Delta[Ca^{2+}]$ = 1 μM, $[Ca^{2+}]_{rest}$ = 50 nM, 34°C) at ~ 0 mV. Buffer capacity κ_{Dye} ([dye] = 100 μM, $[Ca^{2+}]$ = 50 nM, 34°C) are also shown.

Linearity

When $[Ca^{2+}] << K_D$, the fluorescence intensity is proportional to $[Ca^{2+}]$ as defined by Eq. 3 (Fig. 5, red line).

$$\frac{F - F_{min}}{F_{max} - F_{min}} = \frac{[Ca^{2+}]}{K_D} \quad \text{(Eq. 3)}$$

For quantitative experiments, it is best to operate in this linear range. Nonlinearities cause difficulties in quantifying $[Ca^{2+}]$, buffering capacities (see *Endogenous and added buffer* below), and biologically interesting fluctuations in $[Ca^{2+}]$ (*5*, *20*). Nonlinearity (*NL*), defined as the difference (δF) between the linear approximation (Eq. 3) and the exact relationship (Eq. 2), is given by Eq. 4.

$$NL = \frac{\delta F}{(F - F_{min})} = \frac{[Ca^{2+}]}{K_D} \quad \text{(Eq. 4)}$$

Therefore, to limit *NL* to less than 20%, $[Ca^{2+}]$ should not exceed ~ $K_D/5$. Estimates of *NL* under typical experimental conditions are summarized in Table 2. It is possible to use a variety of indicators to measure AP-evoked $\Delta[Ca^{2+}]$, but only low-affinity dyes (Fluo-4FF, X-Rhod-FF, Rhod-FF) are ideal for quantitative measurements of NMDA-mediated changes in $[Ca^{2+}]$. Higher Ca^{2+} indicator concentrations lead to smaller changes in $[Ca^{2+}]$, and therefore also tend to improve linearity at the expense of decreasing SNR (see *choice of indicator* below).

Endogenous and added buffer

Because Ca^{2+} indicators bind Ca^{2+}, they act as Ca^{2+} buffers. The effect of this added buffer on $[Ca^{2+}]$ can be illustrated in terms of a single compartment model (*43, 45, 55*), which is an excellent approximation for small dendrites and spines (*56*). If we assume that $[Ca^{2+}]$ equilibrates rapidly (at typical experimental time resolutions of ~ 1 ms) in the compartment, then the dynamics of changes in $[Ca^{2+}]$ are given by Eq. 5.

$$\frac{d[Ca^{2+}]_T}{dt} = V_{sp}^{-1}\left(i(t) - e(t)\right) \quad \text{(Eq. 5)}$$

The variables $i(t)$ and $e(t)$ indicate Ca^{2+} influx to and efflux from the system, respectively, and V_{sp} is the accessible volume. $[Ca^{2+}]_T$ is the total (bound and free) $[Ca^{2+}]$, and its rate of change can be decomposed as Eq. 6.

$$\frac{d[Ca^{2+}]_T}{dt} = \frac{d[Ca^{2+}]}{dt} + \frac{d[B\,Ca^{2+}]}{dt} + \frac{d[dye\,Ca^{2+}]}{dt} = (1 + \kappa_B + \kappa_{dye})\frac{d[Ca^{2+}]}{dt}$$

(Eq. 6)

$[B\ Ca^{2+}]$ is the concentration of endogenous buffer bound to Ca^{2+}, and Eq. 7 defines the buffer binding ratio (the sub- and superscript X indicates either B or dye).

$$\kappa_X = \frac{\partial[XCa^{2+}]}{\partial[Ca^{2+}]} = \frac{K_D^{(X)}[X]_T}{(K_D^{(X)} + [Ca^{2+}])^2}$$

(Eq. 7)

Thus, $[Ca^{2+}]$ is given as Eq. 8.

$$\frac{d[Ca^{2+}]}{dt} = \frac{1}{\beta V_{sp}}\left(i(t) - e(t)\right)$$

$$\beta = (1 + \kappa_B + \kappa_{dye})$$

(Eq. 8)

Assuming that extrusion is proportional to $([Ca^{2+}] - [Ca^{2+}]_o)$, $e(t) = \Gamma([Ca^{2+}] - [Ca^{2+}]_o)$, where $[Ca^{2+}]_o$ is the resting $[Ca^{2+}]$ and Γ is the extrusion rate constant, the above equation can be solved as Eq. 9 (*21*).

$$[Ca^{2+}] = \int_0^t d\tau \frac{i(\tau)}{\beta V_{sp}} \exp\left[-\frac{\Gamma}{\beta}(t - \tau)\right] + [Ca^{2+}]_o$$

(Eq. 9)

For example, a brief Ca^{2+} current evoked by an action potential at $t = 0$ yields an exponential $[Ca^{2+}]$ transient, defined by Eq. 10.

$$[Ca^{2+}] = \frac{Q}{\beta V_{sp}} \exp\left(-\frac{\Gamma}{\beta}t\right) + [Ca^{2+}]_o$$

(Eq. 10)

In this case, the variable Q is the total amount (moles) of Ca^{2+} transferred. As buffer concentration increases, β increases (Eq. 7 and Eq. 8) and both the peak of the $[Ca^{2+}]$ transient amplitude and the decay rate decrease (Fig. 6A). Approximating NMDAR-mediated currents as $i(t) = (Q\tau_{NMDA}^{-1})^{-t/\tau NMDA}$, the $[Ca^{2+}]$ transient is defined by Eq. 11.

$$[Ca^{2+}] = \frac{Q\beta^{-1}}{V_{sp}\left(1 - \Gamma\beta^{-1}\tau_{NMDA}\right)}\left[\exp\left(-\frac{\Gamma t}{\beta}\right) - \exp\left(-\frac{t}{\tau_{NMDA}}\right)\right] + [Ca^{2+}]_o$$

(Eq. 11)

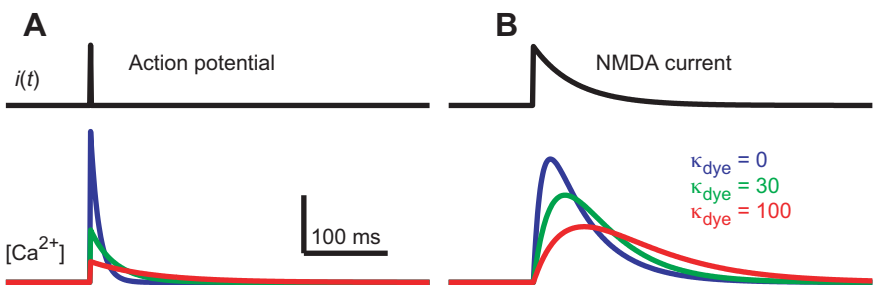

Fig. 6. Buffering effects of added dye on (**A**) AP-evoked and (**B**) synaptic activity-evoked changes in $[Ca^{2+}]$. Curves are derived from Eq. 10 and Eq. 11 (parameters: $\kappa_B = 20$, $\Gamma = 1.6\ ms^{-1}$, $\tau_{NMDA} = 50$ ms).

Note that the attenuation of the amplitude by addition of buffer is smaller for the synaptic stimulus-evoked $[Ca^{2+}]$ transient than for the AP-evoked $[Ca^{2+}]$ transient (Fig. 6B). This difference is largely due to the longer durations of the synaptic currents, which allow the resulting $[Ca^{2+}]$ transients to summate. Nevertheless, it is clear that under the experimental conditions used in most published studies, the indicator severely perturbs $[Ca^{2+}]$ dynamics and dominates endogenous buffers. In hippocampal spines, κ_B is about 20. Therefore, 100 μM OGB-1 or Fluo-4 attenuates the $[Ca^{2+}]$ transient amplitude by a factor of 10 (Table 2). Lower dye concentrations give higher SNR, but also larger NL.

Choice of indicator

The choice of indicator and its concentration should be guided primarily by the scientific goals of the measurement. If one wants to probe the Ca^{2+} dynamics of the neuron as it would be in the absence of the Ca^{2+} indicator, it is important to add low amounts of exogenous buffer compared to the amount of endogenous buffer in the cell ($\kappa_B >> \kappa_{dye}$); alternatively, it may be possible to correct for the presence of the Ca^{2+} indicator (*43, 45, 55, 56*). In contrast, if a quantity proportional to the total Ca^{2+} influx is desirable, high added buffer capacity is necessary, $\kappa_B << \kappa_{dye}$. Additional important factors in choosing an indicator include the SNR and linearity. Low concentrations of high-affinity indicators [for example, 20 μM Fluo-4 (*21*)] give the best SNR, but also suffer from nonlinearities. As a rough guide, we recommend 100 to 300 μM Fluo-4, Fluo-5F, X-Rhod-1, or X-Rhod-5F to measure AP-evoked Ca^{2+} dynamics, and 500 μM Fluo-4FF, X-Rhod-FF, or Rhod-FF for changes in $[Ca^{2+}]$ evoked by synaptic stimulation.

Quantification of $[Ca^{2+}]$ Transients with a Single Indicator

The standard method of monitoring Ca^{2+} dynamics involves a single Ca^{2+} indicator (*15*, *19*, *22*). In the linear regime, the quantity $\Delta F/F_o$ is proportional to the transient changes in Ca^{2+} and does not depend on focal position and geometric factors. However, great care must be taken for the background subtraction and the calibration of Ca^{2+} signal.

Background subtraction

Relating fluorescence and $[Ca^{2+}]$ requires subtraction of background from the fluorescence signal. Because neuronal compartments such as spines and boutons are typically smaller than the excitation volume of 2PLSM (*57, 58*), the background calculation is complicated. Background fluorescence is commonly estimated by measuring fluorescence far from the spine, F_B. $\Delta F/F_o$ is defined by Eq. 12, where F and $F_{o,\,raw}$ are the raw fluorescence signals during the response and baseline periods.

$$\frac{\Delta F}{F_o} = \frac{F - F_{o,raw}}{F_{o,raw} - F_B} \qquad \text{(Eq. 12)}$$

Because the spine volume is smaller than the excitation volume, F, F_o, F_{raw}, and F_B can be expressed by Eq. 13, where V_{sp} and V_{ex} are the spine volume and the excitation volume outside the compartment, b_{sp} and b_{ex} are background fluorescence intensities inside and outside the compartment per unit volume, respectively, and f_o and f are the fluorescence intensities from fluorophore in the compartment per unit volume before and after the stimulation.

$$\begin{aligned} F &= (f + b_{sp})V_{sp} + b_{ex}V_{ex} \\ F_{o,\,raw} &= (f_o + b_{sp})V_{sp} + b_{ex}V_{ex} \\ F_B &= b_{ex}(V_{sp} + V_{ex}) \end{aligned} \qquad \text{(Eq. 13)}$$

Because the excitation volume is $V_{sp}+ V_{ex}$, $\Delta F/F_o$ is defined by Eq. 14.

$$\frac{\Delta F}{F_o} = \frac{(f - f_o)}{f_o - (b_{ex} - b_{sp})}$$

(Eq. 14)

Therefore, this type of background subtraction gives the correct value only if $b_{sp} = b_{ex}$, that is, if background is exactly the same inside and outside spine. Unfortunately, this is rarely the case. Under some conditions, depending on the excitation wavelength, spatially heterogeneous background fluorescence is excited. More importantly, it is often the case that small quantities of indicator spilled in the extracellular space during patching produce substantial background fluorescence in the brain slice. In this case, background subtraction always results in an underestimate of F_o and a resulting overestimate of $\Delta F/F_o$. Moreover, this error depends on the size of the compartment; it is larger for smaller compartments. In our view, quantitative measurements demand conditions in which the background is not significantly different from the dark noise of the PMT. If background fluorescence is higher than the dark noise of the PMT, the data are severely compromised for analysis of the amplitudes and time-courses of transient changes in $[Ca^{2+}]$ (*21*).

Calibrating [Ca²⁺] signals

To calibrate fluorescence changes in terms of absolute Ca^{2+} concentrations, further steps are required. Assuming $[Ca^{2+}]_o$ is approximately 50 nM, the amplitudes of transient changes in $[Ca^{2+}]$ can be easily estimated. However, $[Ca^{2+}]_o$ differs from cell to cell and depends on subcellular location (*21*) and neuronal health (*46*). Under some conditions, a more robust and precise estimate of $[Ca^{2+}]$ can be calculated (*46*) by Eq. 15.

$$\frac{[Ca^{2+}]}{K_D} = \frac{F / F_{max} - F_{min} / F_{max}}{1 - F / F_{max}}$$

(Eq. 15)

F_{min}/F_{max} can be estimated in cuvette experiments (Table 2), and for large dynamic-range indicators, the exact value is not required. However, F_{max} needs to be estimated quantitatively in situ, for example, using trains of action potentials (*46*).

Quantification of [Ca²⁺] Transients with Dual Indicators

The interpretation of Ca^{2+} imaging experiments greatly benefits from the use of two fluorophores with emission wavelengths that are spectrally separable. This approach is especially useful in the case of 2PLSM, because their broad two-photon cross sections (*59*) allow the simultaneous excitation of two or more fluorophores with vastly different emission wavelengths (Figs. 2 and 3). For Ca^{2+} imaging experiments, one of the fluorophores is Ca^{2+}-sensitive (typically green, *G*) and the other is Ca^{2+}-insensitive (typically red, *R*) (*5*, *18*). The ratio $\Delta G/R$ is then a measure of $[Ca^{2+}]$.

The dual indicator method has several advantages. First, for the Ca^{2+}-insensitive dye, relatively high concentrations of bright fluorophore can be used, which aids in locating small structures such as dendritic spines (Figs. 2 and 3). Second, the denominator in $\Delta G/R$ is large and can be integrated over the entire imaging trial. For example, with an excitation of 810 nm, 20 to 40 μM Alexa-594 produces more than 20 times the photons produced by 100 μM Fluo-4. $\Delta G/R$ is therefore a substantially less noisy estimate of $[Ca^{2+}]$ than $\Delta F/F_o$. Third, $\Delta G/R$ is relatively insensitive to background fluorescence. ΔG does not depend on a background measurement, and several factors conspire to make the estimate of *R* robust: (i) *R* is a large signal; (ii) Ca^{2+}-insensitive dyes tend to be less "sticky" in the extracellular space; and (iii) there is little autofluorescence in the tissue at red wavelengths. Fourth, the dual indicator method is insensitive to changes in baseline fluorescence due to fluctuations in $[Ca^{2+}]_o$. These fluctuations cause fluctuations in $\Delta G/G_o$, which can be mistaken for fluctuations in $[Ca^{2+}]$ transients. $\Delta G/R$ is much less susceptible to this error (Fig. 7). Fifth, measuring G_o/R is an excellent gauge of $[Ca^{2+}]_o$ and cell health.

Using the dual indicator method $[Ca^{2+}]$ can be measured by Eq. 16 (*5*)

$$\frac{[Ca^{2+}]}{K_D} = \frac{(G/R) - (G/R)_{min}}{(G/R)_{max} - (G/R)}$$

(Eq. 16)

Alternatively, in the linear regime ($[Ca^{2+}] << K_D$), $[Ca^{2+}]$ can be measured by Eq. 17.

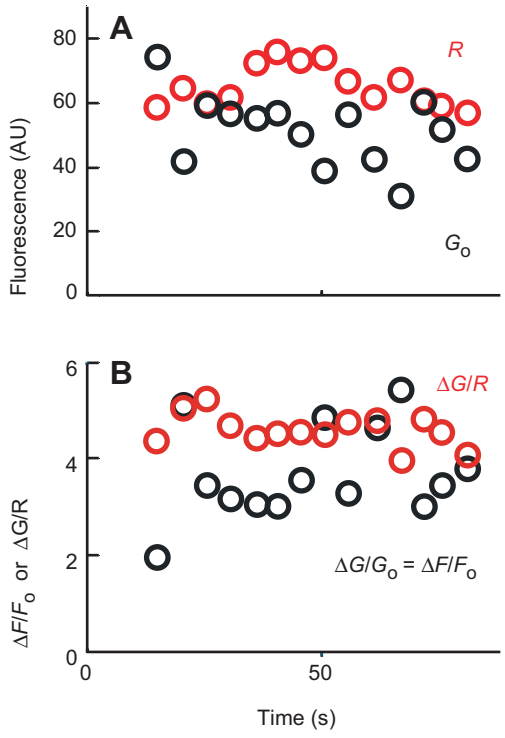

Fig. 7. Fluorescence transients in response to synaptic stimulation. (**A**) Baseline fluctuations for the Ca^{2+}-sensitive (G_o) and Ca^{2+}-insensitive (R) signal. Note the large fluctuations in baseline fluorescence G_o (black circles), presumably due to fluctuations in resting Ca^{2+} concentration, $[Ca^{2+}]_o$. Red fluorescence (R, red circles) is more stable. (**B**) As a result of the baseline fluctuations, synaptically evoked fluorescence transients computed as $\Delta G/G_o$ show large fluctuations. Therefore, in single-indicator experiments these baseline fluctuations reduce the SNR and pollute estimates of biologically interesting fluctuations. The dual-indicator estimate $\Delta G/R$ is several-fold less noisy.

$$\frac{[Ca^{2+}]}{K_D} = \frac{(G/R) - (G/R)_{min}}{(G/R)_{max} - (G/R)_{min}}$$

(Eq. 17)

$(G/R)_{max}$ and $(G/R)_{min}$ are the green:red ratios under saturating and zero $[Ca^{2+}]$ conditions, measured in a pipette containing the fluorophore mixture plus 2 mM Ca^{2+} or 2 mM EGTA (in practice, be sure to adjust the pH), respectively. Note that the values of G/R depend on factors other than $[Ca^{2+}]$, including particular optics and detectors, batches of indicator, and other factors. Therefore, for absolute measurements of $[Ca^{2+}]$, or in cases where values of $\Delta G/R$ are to be compared over extended times, routine measurements of $(G/R)_{max}$ and $(G/R)_{min}$ are essential.

We typically use the green fluorescent Ca^{2+}-sensitive indicators Fluo-4, Fluo-5F, and Fluo-4FF, and the red fluorescent Ca^{2+}-insensitive fluorophore Alexa-594 (*5*, *18*). It is also possible to use the opposite spectral configuration: For example, the green fluorescent Ca^{2+}-insensitive fluorophore Alexa-488 and the red fluorescent Ca^{2+}-sensitive indicator X-Rhod 1, X-Rhod-5F, X-Rhod-FF, or Rhod-FF (*53*). All of these fluorophores can be efficiently excited at 810 nm or 910 nm, and red and green fluorescence can be separated with dichroic mirrors and bandpass filters with negligible cross talk (Fig. 1).

Pharmacologic Analyses of $[Ca^{2+}]$ Transients

The molecular sources of Ca^{2+} can be dissected pharmacologically in Ca^{2+} imaging experiments (*5*, *20*). However, the fact that indicators attenuate the amplitudes of transient changes in $[Ca^{2+}]$ makes pharmacologic analysis challenging. This is especially true for drugs that interfere with the function of voltage-gated Ca^{2+} channels (for example, dyhydropyridines, agatoxins, and conotoxins), which often equilibrate slowly. If the concentration of the Ca^{2+} indicator increased during drug application, an attenuation of the change in $[Ca^{2+}]$ would be observed even if the Ca^{2+} influx were not affected by the drug. It is, therefore, very important to allow for complete indicator equilibration, often requiring more than 30 to 40 min of baseline recording even when recording close (<150 μm) to the cell body (*21*). Testing for diffusional equilibration is best done by online data analysis, measuring, for example, the time-dependent increase of the Ca^{2+}-insensitive fluorescence channel (*21*, *45*, *46*).

References and Notes

1. J. A. Cummings, R. M. Mulkey, R. A. Nicoll, R. C. Malenka, Ca^{2+} signaling requirements for long-term depression in the hippocampus. *Neuron* **16**, 825–833 (1996).
2. R. C. Malenka, R. A. Nicoll, Long-term potentiation—a decade of progress? *Science* **285**, 1870–1874 (1999).
3. T. Budde, S. Meuth, H. C. Pape, Calcium-dependent inactivation of neuronal calcium channels. *Nat. Rev. Neurosci.* **3**, 873–883 (2002).
4. J. P. Imredy, D. T. Yue, Mechanism of Ca^{2+}-sensitive inactivation of L-type Ca^{2+} channels. *Neuron* **12**, 1301–1318 (1994).
5. R. Yasuda, B. L. Sabatini, K. Svoboda, Plasticity of calcium channels in dendritic spines. *Nat. Neurosci.* **6**, 948–955 (2003).
6. W. C. Sin, K. Haas, E. S. Ruthazer, H. T. Cline, Dendrite growth increased by visual activity requires NMDA receptor and Rho GTPases. *Nature* **419**, 475–480 (2002).
7. F. Engert, T. Bonhoeffer, Dendritic spine changes associated with hippocampal long-term synaptic plasticity. *Nature* **399**, 66–70 (1999).
8. M. Maletic-Savatic, R. Malinow, K. Svoboda, Rapid dendritic morphogenesis in CA1 hippocampal dendrites induced by synaptic activity. *Science* **283**, 1923–1927 (1999).
9. P. Vanhoutte, H. Bading, Opposing roles of synaptic and extrasynaptic NMDA receptors in neuronal calcium signalling and BDNF gene regulation. *Curr. Opin. Neurobiol.* **13**, 366–371 (2003).
10. K. Svoboda, D. W. Tank, W. Denk, Direct measurement of coupling between dendritic spines and shafts. *Science* **272**, 716–719 (1996).
11. B. S. Sabatini, T. G. Oertner, K. Svoboda, The life cycle of Ca^{2+} ions in dendritic spines. *Neuron* **33**, 439–452 (2002).
12. A. Majewska, E. Brown, J. Ross, R. Yuste, Mechanisms of calcium decay kinetics in hippocampal spines: Role of spine calcium pumps and calcium diffusion through the spine neck in biochemical compartmentalization. *J. Neurosci.* **20**, 1722–1734 (2000).
13. H. Schmidt, E. B. Brown, B. Schwaller, J. Eilers, Diffusional mobility of parvalbumin in spiny dendrites of cerebellar Purkinje neurons quantified by fluorescence recovery after photobleaching. *Biophys. J.* **84**, 2599–2608 (2003).
14. W. Muller, J. A. Connor, Dendritic spines as individual neuronal compartments for synaptic Ca^{2+} responses. *Nature* **354**, 73–76 (1991).
15. Z. F. Mainen, R. Malinow, K. Svoboda, Synaptic calcium transients in single spines indicate that NMDA receptors are not saturated. *Nature* **399**, 151–155 (1999).
16. R. Yuste, A. Majewska, S. S. Cash, W. Denk, Mechanisms of calcium influx into hippocampal spines: heterogeneity among spines, coincidence detection by NMDA receptors, and optical quantal analysis. *J. Neurosci.* **19**, 1976–1987 (1999).
17. Y. Kovalchuk, J. Eilers, J. Lisman, A. Konnerth, NMDA receptor-mediated subthreshold Ca^{2+} signals in spines of hippocampal neurons. *J. Neurosci.* **20**, 1791–1799 (2000).
18. T. G. Oertner, B. S. Sabatini, E. A. Nimchinsky, K. Svoboda, Facilitation at single synapses probed with optical quantal analysis. *Nat. Neurosci.* **5**, 657–664 (2002).
19. R. Yuste, W. Denk, Dendritic spines as basic functional units of neuronal integration. *Nature* **375**, 682–684 (1995).
20. B. L. Sabatini, K. Svoboda, Analysis of calcium channels in single spines using optical fluctuation analysis. *Nature* **408**, 589–593 (2000).
21. B. L. Sabatini, M. Maravall, K. Svoboda, Ca^{2+} signaling in dendritic spines. *Curr. Opin. Neurobiol.* **11**, 349–356 (2001).
22. M. Umemiya, M. Senda, T. H. Murphy, Behaviour of NMDA and AMPA receptor-mediated miniature EPSCs at rat cortical neuron synapses identified by calcium imaging. *J. Physiol.* **521**, 113–122 (1999).
23. H. J. Koester, B. Sakmann, Calcium dynamics in single spines during coincident pre- and postsynaptic activity depend on relative timing of back-propagating action potentials and subthreshold excitatory postsynaptic potentials. *Proc. Natl. Acad. Sci. U.S.A.* **95**, 9596–9601 (1998).
24. E. A. Nimchinsky, R. Yasuda, T. Oertner, K. Svoboda, *J. Neurosci.*, in press.
25. W. Denk, J. H. Strickler, W. W. Webb, Two-photon laser scanning fluorescence microscopy. *Science* **248**, 73–76 (1990).
26. W. Denk, K. Svoboda, Photon upmanship: Why multiphoton imaging is more than a gimmick. *Neuron* **18**, 351–357 (1997).
27. B. Sakmann, G. Stuart, in *Single-Channel Recording*, B. Sakmann and E. Neher, Eds. (Plenum, New York, 1995),. pp. 199–211.
28. A. Konnerth, A. L. Obaid, B. M. Salzberg, Optical recording of electrical activity from parallel fibres and other cell types in skate cerebellar slices in vitro. *J. Physiol.* **393**, 681–702 (1987).
29. A. Majewska, G. Yiu, R. Yuste, A custom-made two-photon microscope and deconvolution system. *Pflugers Arch.* **441**, 398–408 (2000).
30. Z. F. Mainen, M. Maletic-Savatic, S. H. Shi, Y. Hayashi, R. Malinow, K. Svoboda, Two-photon imaging in living brain slices. *Methods* **18**, 231–239 (1999).
31. T. Pologruto, B. L. Sabatini, K. Svoboda, ScanImage: Flexible software for operating laser scanning microscopes. *Biomed. Eng. Online* **2**, 13 (2003).
32. H. U. Dodt, M. Eder, A. Schierloh, W. Zieglgänsberger, Infrared-guided laser stimulation of neurons in brain slices. *Sci. STKE* **2002** pl2 (2002).
33. J. C. Callaway, W. N. Ross, Frequency-dependent propagation of sodium action potentials in dendrites of hippocampal CA1 pyramidal neurons. *J. Neurophysiol.* **74**, 1395–1403 (1995).
34. R. S. Zucker, W. G. Regehr, Short-term synaptic plasticity. *Annu. Rev. Physiol.* **64**, 355–405 (2002).
35. L. Wu, C. S. Bauer, X. G. Zhen, C. Xie, J. Yang, Dual regulation of voltage-gated calcium channels by PtdIns(4,5)P2. *Nature* **419**, 947–952 (2002).
36. A. J. Berger, S. Dieudonne, P. Ascher, Glycine uptake governs glycine site occupancy at NMDA receptors of excitatory synapses. *J. Neurophysiol.* **80**, 3336-3340 (1998).
37. W. G. Regehr, D. W. Tank, Selective fura-2 loading of presynaptic terminals and nerve cell processes by local perfusion in mammalian brain slice. *J. Neurosci. Methods* **37**, 111–119 (1991).
38. R. Yuste, A. Peinado, L. C. Katz, Neuronal domains in developing neocortex. *Science* **257**, 665–669 (1992).
39. O'Malley, Y.-H. Kao, J. R. Fetcho, Imaging the functional organization of zebrafish hindbrain segments during escape behaviors. *Neuron* **17**, 1145-1155 (1996).
40. K. Delaney, I. Davison, W. Denk, Odour-evoked $[Ca^{2+}]$ transients in mitral cell dendrites of frog olfactory glomeruli. *Eur. J. Neurosci.* **13**, 1658-1672 (2001).
41. D. W. Tank, M. Sugimori, J. A. Connor, R. R. Llinas, Spatially resolved calcium dynamics of mammalian Purkinje cells in cerebellar slice. *Science* **242**, 773-777 (1988).
42. K. Svoboda, W. Denk, D. Kleinfeld, D. W. Tank, In vivo dendritic calcium dynamics in neocortical pyramidal neurons. *Nature* **385**, 161–165 (1997).
43. E. Neher, G. J. Augustine, Calcium gradients and buffers in bovine chromaffin cells. *J. Physiol.* **450**, 273–301 (1992).
44. E. Neher, The use of fura-2 for estimating Ca buffers and Ca fluxes. *Neuropharmacology* **34**, 1423–1442 (1995).
45. F. Helmchen, K. Imoto, B. Sakmann, Ca^{2+} buffering and action potential-evoked Ca^{2+} signaling in dendrites of pyramidal neurons. *Biophys. J.* **70**, 1069–1081 (1996).
46. M. Maravall, Z. M. Mainen, B. L. Sabatini, K. Svoboda, Estimating intracellular calcium concentrations and buffering without wavelength ratioing. *Biophys. J.* **78**, 2655–2667 (2000).
47. R. Y. Tsien, Fluorescent probes of cell signaling. *Annu. Rev. Neurosci.* 12, 227–253 (1989).
48. G. Grynkiewicz, M. Poenie, R. Y. Tsien, A new generation of Ca^{2+} indicators with greatly improved fluorescence properties. *J. Biol. Chem.* **260**, 3440–3450 (1985).
49. A. Frick, J. Magee, H. J. Koester, M. Migliore, D. Johnston, Normalization of Ca^{2+} signals by small oblique dendrites of CA1 pyramidal neurons. *J. Neurosci.* **23**, 3243–3250 (2003).
50. R. Tsien, T. Pozzan, Measurement of cytosolic free Ca^{2+} with quin2. *Methods Enzymol.* **172**, 230–262 (1989).
51. D. M. Bers, C. W. Patton, R. Nuccitelli, A practical guide to the preparation of Ca^{2+} buffers. *Methods Cell Biol.* **40**, 3–29 (1994).
52. A. B. Harkins, N. Kurebayashi, S. M. Baylor, Resting myoplasmic free calcium in frog skeletal muscle fibers estimated with fluo-3. *Biophys. J.* **65**, 865–881 (1993).
53. T. A. Pologruto, R. Yasuda, K. Svoboda, unpublished data.
54 D. M. O'Malley, B. Burbach, P. Adams, in *Confocal Microscopy Methods and Protocols*, S. Paddock, Ed. (Humana Press, New York, 1999), vol. 122, pp. 261–303.
55. W. B. Busa, Spectral characterization of the effect of viscosity on Fura-2 fluorescence: Excitation wavelength optimization abolishes the viscosity artifact. *Cell Calcium* **13**, 313–319 (1992).

56. D. W. Tank, W. G. Regehr, K. R. Delaney, A quantitative analysis of presynaptic calcium dynamics that contribute to short-term enhancement. *J. Neurosci.* **15**, 7940–7952 (1995).
57. B. L. Sabatini, W. G. Regehr, Optical measurement of presynaptic calcium currents. *Biophys. J.* **74**, 1549–1563 (1998).
58. K. M. Harris, F. E. Jensen, B. Tsao, Three-dimensional structure of dendritic spines and synapses in rat hippocampus (CA1) at postnatal day 15 and adult ages: Implications for the maturation of synaptic physiology and long-term potentiation. *J. Neurosci.* **12**, 2685–2705 (1992).
59. G. M. Shepherd, K. M. Harris, Three-dimensional structure and composition of CA3—>CA1 axons in rat hippocampal slices: Implications for presynaptic connectivity and compartmentalization. *J. Neurosci.* **18**, 8300–8310 (1998).
60. C. Xu, W. Zipfel, J. B. Shear, R. M. Williams, W. W. Webb, Multiphoton fluorescence excitation: New spectral windows for biological nonlinear microscopy. *Proc. Natl. Acad. Sci. U.S.A.* **93**, 10763–10768 (1996).
61. H. U. Dodt, A. Frick, K. Kampe, W. Zieglgänsberger, NMDA and AMPA receptors on neocortical neurons are differentially distributed. *Eur. J. Neurosci.* **10**, 3351–3357 (1998).
62. H. U. Dodt, A. Schierloh, M. Eder, W. Zieglgänsberger, Circuitry of rat barrel cortex investigated by infrared-guided laser stimulation. *Neuroreport* **14**, 623–627 (2003).
63. We thank Alla Karpova and Aleksander Sobczyk for a critical reading of the manuscript, members of our laboratory for discussions, and Barry J. Burbach and Peter O'Brien for technical help. This work was supported by Burroughs Wellcome Fund (R.Y., B.L.S.), NIH (E.A.N.), Human Frontier Science Program (V.S.), Howard Hughes Medical Institute, and NIH.

Citation: R. Yasuda, E. A. Nimchinsky, V. Scheuss, T. A. Pologruto, T. G. Oertner, B. L. Sabatini, K. Svoboda, Imaging calcium concentration dynamics in small neuronal compartments. Sci. *STKE* **2004**, pl5 (2004).